International Forum on Aeroelasticity and Structural Dynamics
IFASD 2024
17-21 June 2024, The Hague, The Netherlands

WHIRL FLUTTER ANALYSIS USING LINEARIZED PROPELLER TRANSFER MATRICES

Christopher Koch[1]

[1]Institute of Aeroelasticity, German Aerospace Center (DLR)
Bunsenstraße 10, 37073 Göttingen, Germany
christopher.koch@dlr.de

Keywords: aeroelasticity, flutter, whirl flutter, propeller, turboprop aircraft

Abstract: Whirl flutter as an aeroelastic instability can occur for aircraft configurations with propellers mounted on an elastic support. It has to be mitigated in the design process, and its prediction needs to be included in the frequency-domain flutter analysis process of such aircraft. But, as these processes often rely on the classical method developed by Houbolt and Reed and revolve around linear aerodynamic derivatives for the propeller, they are not always compatible with advanced frequency-domain representations of the propeller such as the Transfer-Matrix method. This paper provides a linearization procedure to derive propeller aerodynamic derivatives similar to those from the classical method from frequency-dependent transfer matrices. These linearized derivatives are compatible with legacy workflows and allow an increase in the fidelity of propeller aerodynamics in existing frequency-domain flutter workflows. This paper also compares the impact of different propeller aerodynamic modeling on the whirl flutter stability of a generic, twin-engine turboprop aircraft. Results show the linearized workflow's effectiveness and indicate a stabilizing effect when including more modeling features like unsteady aerodynamics and local induced velocities.

1 INTRODUCTION

Since the 1960s and two crashes of the Lockheed L-188 Electra [1] caused by an aeroelastic instability called whirl flutter, including the motion-induced loads of a rotating propeller is mandatory for turboprop aircraft flutter analysis [2]. A standard method used in literature to compute the aerodynamic transfer functions from propeller hub motion to hub loads is the method developed by Houbolt and Reed [3]. Rodden and Rose reformulated that method into a form compatible with frequency-domain flutter analysis, e.g., in MSC Nastran [4]. The method uses aerodynamic derivatives to describe the motion-induced loads. It is fast and easy to apply, so the workflow has become a workhorse for different application purposes. It is suitable for broad parameter studies [5–7], for exploring the effect of individual modeling aspects on whirl flutter [8], and is used for certification [9]. However, it has some shortcomings due to its analytical character. The derivation of the aerodynamic derivative is based on a strip-theory approach and only considers linear perturbational terms for the lift, neglecting the steady state. It does not consider induced velocities and unsteady lift-lag effects. The latter are only approximated. To summarize, the aerodynamic model is simplified, and the derivation can not be extended easily. Literature provides other methods to obtain aerodynamic derivatives with fewer assumptions. Wang and Chen [10] propose low-frequency, quasi-steady harmonic perturbations in conjunction with an unsteady vortex lattice method (UVLM) to identify instead of analytically derive the transfer functions. While capturing the quasi-steady part of the transfer behavior using a

more sophisticated aerodynamic model, their method still does not fully account for unsteady aerodynamics. Gennaretti and Greco [11] present a procedure to identify a finite-state reduced-order model (ROM) for different unsteady aerodynamic models of a prop-rotor. In their study of the whirl flutter stability of a simplified two-degree-of-freedom (DOF) pylon system, they compare different low- and mid-fidelity aerodynamic methods for rotors with varying numbers of blades and aspect ratios. For high advance ratios, their study shows an under-prediction of whirl flutter stability by the low-fidelity methods compared to the mid-fidelity method. However, their procedure is embedded into the aerodynamic solver on the equation level, making it a bit more challenging to extend to other solvers.

The author proposed the Transfer-Matrix method (or TM-method) [12] to overcome existing approaches' shortcomings and allow including arbitrary time-domain models of an isolated propeller into frequency-domain flutter analyses. Opposed to the method proposed by Wang and Chen, the TM-method identifies the complete frequency-dependent transfer behavior of the time-domain propeller model, inherently capturing effects from unsteady aerodynamics and even blade elasticity [13]. Koch, Böhnisch, et al. [14] applied this procedure to study the unsteady aerodynamics of an turboprop propeller and, consequently, the whirl flutter stability of a two-DOF pylon system. The study compares low- and mid-fidelity methods, from quasi-steady strip theory to 3D panel free-wake codes. The results reveal a good fit for the unsteady aerodynamic loads, where the mid-fidelity methods show a good correlation, and the strip-theory methods predict higher unsteady loads if induced velocities and unsteady aerodynamics are neglected. However, trends for whirl flutter stability do not follow the clear trends for unsteady aerodynamics. The authors show that for the simplified pylon model, the relative scaling of the different aerodynamic derivatives is more critical than the absolute values. Over-predicting all derivatives results in a cancellation of errors, as stabilizing and destabilizing derivatives balance each other. On the other hand, a slight over-prediction of a stabilizing derivative relative to the others has a much higher impact on whirl flutter stability. This sensitivity makes it hard to generalize the results, as no clear trends could be observed for whirl flutter stability. Results show that they depend on airframe parameters such as the mode shape.

This paper aims to extend these studies concerning the impact of propeller aerodynamics on whirl flutter stability to a full aircraft level to see whether the unclear trends also prevail on the more complex model. Especially the (damping) influence of wing aerodynamics might reduce the sensitivity of the flutter speed concerning the stabilizing propeller derivatives. Additionally, the paper presents a linearization procedure for the frequency-dependent propeller transfer matrices. This allows obtaining aerodynamic derivatives compatible with legacy whirl flutter workflows and including the relevant unsteady aerodynamic terms.

First, this paper briefly reviews the theory for frequency-domain whirl flutter, including the TM-method. Further, the aerodynamic methods considered in the present study are reviewed. In the following sections, the propeller and airframe models are presented. The aircraft model is developed and used in a parallel study by Noël et al. [15] on the influence of blade elasticity. The present paper completely neglects blade elasticity and focuses on propeller aerodynamics. The results in the next section comprise a look at the aerodynamic derivatives, both in detail for one operating point and over the airspeed range, and frequency and damping plots. The latter compare different aerodynamic methods and the original TM-method to the linearized approaches. Finally, the last section summarizes and discusses the results.

2 THEORY

The following section briefly describes the general methodology of frequency-domain flutter analysis with additional contributions of unsteady loads due to propeller aerodynamics and gyroscopics. The legacy Houbolt/Reed method and the Transfer-Matrix method are summarized, but the focus is on the linearization procedure to obtain propeller aerodynamic derivatives compatible with the legacy workflow by Houbolt and Reed. Finally, a brief overview of the methods used for aerodynamic modeling of the propeller is given, too.

2.1 Frequency-domain whirl flutter analysis

The generalized equations of motion for an aeroelastic aircraft with stiffness, damping, and mass from the aircraft structure ($\underline{K}_{gen}$, $\underline{D}_{gen}$ and $\underline{M}_{gen}$), unsteady aerodynamic forces from the aircrafts lifting surfaces ($\frac{\rho}{2}V^2\underline{Q}_{gen}(k, Ma)$) and unsteady, motion-induced hub loads from the propeller are given in Eq. 1 [12]. The equations are formulated for generalized coordinates $\boldsymbol{q}$.

$$\left[s^2\underline{M}_{gen} + s\underline{D}_{gen} + \underline{K}_{gen}\right]\boldsymbol{q} \;=\; \frac{\rho}{2}V^2\underline{Q}_{gen}(k, Ma)\boldsymbol{q} \;+\; \underline{\Phi}^T_{prop}\underline{H}_{prop}(s, V, \Omega, Ma)\underline{\Phi}_{prop}\boldsymbol{q} \quad (1)$$

The motion-induced propeller hub loads are described by a linear transfer matrix $\underline{H}_{prop}$ in the Laplace domain, connecting the motion at the propeller hub node $\Delta\boldsymbol{x}_{hub}$ with the respective hub loads $\boldsymbol{F}_{prop,hub}$, as shown in Eq. 2. The unsteady hub forces are transformed into generalized coordinates using the modal matrix for the propeller hub node $\underline{\Phi}_{prop}$, which projects the generalized coordinates onto the physical displacements of the propeller hub and vice versa [12].

$$\boldsymbol{F}_{prop,hub} \;=\; \underline{H}_{prop}(s, V, \Omega, Ma)\;\Delta\boldsymbol{x}_{hub} \quad (2)$$

An analytical derivation of the unsteady aerodynamics of a propeller in axial flight was developed by Houbolt and Reed [3]. The Houbolt/Reed method describes the motion-induced propeller hub forces in terms of analytically derived, non-dimensional stiffness and damping derivatives, which can be sorted into a stiffness and damping matrix as shown in Eq. 3-4. The derivative C_{ab} gives the perturbation response of the hub load component a for the perturbation in direction b. Analytical formulas for the derivatives can be found in the literature [3, 4, 16].

$$\underline{H}_{prop}(s, V, \Omega, Ma) \;=\; \pi R^3\rho V^2(\underline{K}_{prop} + s\underline{D}_{prop}) \quad (3)$$

$$\underline{K}_{prop} \;=\; \begin{bmatrix} 0 & 0 & 0 & 0 & 0 & 0 \\ 0 & 0 & 0 & 0 & \frac{C_{y\theta}}{2R} & \frac{C_{y\psi}}{2R} \\ 0 & 0 & 0 & 0 & \frac{C_{z\theta}}{2R} & \frac{C_{z\psi}}{2R} \\ 0 & 0 & 0 & 0 & 0 & 0 \\ 0 & 0 & 0 & 0 & C_{m\theta} & C_{m\psi} \\ 0 & 0 & 0 & 0 & C_{n\theta} & C_{n\psi} \end{bmatrix} ;\; \underline{D}_{prop} \;=\; \begin{bmatrix} 0 & 0 & 0 & 0 & 0 & 0 \\ 0 & -\frac{C_{y\psi}}{2RV} & \frac{C_{y\theta}}{2RV} & 0 & \frac{C_{yq}}{2V} & \frac{C_{yr}}{2V} \\ 0 & -\frac{C_{z\psi}}{2RV} & \frac{C_{z\theta}}{2RV} & 0 & \frac{C_{zq}}{2V} & \frac{C_{zr}}{2V} \\ 0 & 0 & 0 & 0 & 0 & 0 \\ 0 & -\frac{C_{m\psi}}{V} & \frac{C_{m\theta}}{V} & 0 & \frac{C_{mq}R}{V} & \frac{C_{mr}R}{V} \\ 0 & -\frac{C_{n\psi}}{V} & \frac{C_{n\theta}}{V} & 0 & \frac{C_{nq}R}{V} & \frac{C_{nr}R}{V} \end{bmatrix} \quad (4)$$

In addition to the unsteady aerodynamics, the gyroscopic torques due to the tilting of the propeller axis must be considered. They lead to a skew-symmetric damping matrix $\underline{G}$, with the polar moment of inertia of the propeller (and engine) I_p and the shaft speed Ω.

$$\underline{H}_{prop}(s,\Omega) \;=\; s\underline{G}(\Omega) \;=\; s\begin{bmatrix} 0 & 0 & 0 & 0 & 0 & 0 \\ 0 & 0 & 0 & 0 & 0 & 0 \\ 0 & 0 & 0 & 0 & 0 & 0 \\ 0 & 0 & 0 & 0 & 0 & 0 \\ 0 & 0 & 0 & 0 & 0 & -I_p\Omega \\ 0 & 0 & 0 & 0 & I_p\Omega & 0 \end{bmatrix} \tag{5}$$

The transfer matrices from gyroscopics and unsteady aerodynamics can be summed to obtain the aeroelastic transfer matrix for each propeller. The equations of motion in Eq. 1 are solved in a final step for the eigenvalues of the aeroelastic system. Because Eq. 1 includes frequency-dependent terms as well as terms that are (explicitly or implicitly) dependent on the operating point (airspeed, shaft speed), the eigenvalues are extracted over the whole operating range using classical flutter solvers like the pk-method [17] or the g-method [18]. Commercial aeroelastic software packages such as ZAERO [19] or Nastran [20] include interfaces to automate the process of considering operating-point-dependent propeller transfer functions.

2.2 Transfer-Matrix method

Instead of analytically deriving $\underline{H}_{prop}$, the Transfer-Matrix method (or TM-method) is developed around the idea of identifying the linear, frequency-domain transfer functions from hub motion to hub loads from an isolated time-domain propeller model. This yields scalar transfer functions, which are (nonlinearly) dependant on the frequency $i\omega$ and can be assembled into the transfer matrices as shown in Eq. 6. For more details on the TM-method, the reader can refer to the literature [12–14].

$$\underline{H}_{prop}(i\omega, V, \Omega, Ma) \;=\; \begin{bmatrix} F_{xx} & F_{xy} & F_{xz} & F_{x\phi} & F_{x\theta} & F_{x\psi} \\ F_{yx} & F_{yy} & F_{yz} & F_{y\phi} & F_{y\theta} & F_{y\psi} \\ F_{zx} & F_{zy} & F_{zz} & F_{z\phi} & F_{z\theta} & F_{z\psi} \\ M_{xx} & M_{xy} & M_{xz} & M_{x\phi} & M_{x\theta} & M_{x\psi} \\ M_{yx} & M_{yy} & M_{yz} & M_{y\phi} & M_{y\theta} & M_{y\psi} \\ M_{zx} & M_{zy} & M_{zz} & M_{z\phi} & M_{z\theta} & M_{z\psi} \end{bmatrix} \tag{6}$$

The TM-method has been adapted and improved to apply it on full-aircraft level. The additions are presented in parallel to this paper by Noël et al. [15]. However, the transfer matrices remain frequency-dependent and operating-point dependent, posing a challenge to classical whirl flutter workflows built around the operating-point dependent but frequency-invariant Houbolt/Reed derivatives.

2.3 Linearization of transfer matrices with respect to frequency

For some applications, it is beneficial to keep the derivative-based workflow of the Houbolt/Reed method but still improve the aeroelastic transfer function for the propeller, e.g., by considering an improved aerodynamic model compared to the linearized strip theory of Houbolt and Reed. This can be achieved by using the TM-method to identify a set of frequency-dependent transfer matrices $\underline{H}_{prop}(i\omega_k)$ using a time-domain propeller model and linearizing them with respect to frequency into a form similar to Eq. 3. Instead of using the full frequency-dependent set of transfer matrices, two samples are picked to obtain the zero-frequency component and the transfer functions' slope with respect to frequency (compare Eq. 7). The first is equivalent to the aerodynamic stiffness from the Houbolt/Reed method, and the latter corresponds to aerodynamic damping. The tilde on $\underline{\tilde{K}}_{prop}$ and $\underline{\tilde{D}}_{prop}$ indicates that they are still dimensional compared to Eq. 4.

$$\underline{H}_{prop,lin}(i\omega) = \underbrace{\underline{H}_{prop}(0)}_{\underline{\tilde{K}}_{prop}} + \underbrace{\frac{\underline{H}_{prop}(i\omega_1) - \underline{H}_{prop}(0)}{i\omega_1}}_{\underline{\tilde{D}}_{prop}} i\omega \tag{7}$$

In general, the transfer matrices $\underline{H}_{prop}(i\omega_k)$ are complex-valued for $\omega_k > 0$. For this reason, $\underline{\tilde{D}}_{prop}$ is most-likely complex valued, too. The real part of $\underline{\tilde{D}}_{prop}$ corresponds to the classical aerodynamic damping, which is also contained in the theory by Houbolt and Reed. The additional imaginary part can either be neglected (to stay consistent with the Houbolt/Reed method) or retained to better approximate the frequency-dependent character of the transfer functions. Fig. 1 compares the original, frequency-dependent transfer function and the real and complex linearisations, linearized about $\omega_1 = 10Hz$. The complex linearisation better approximates the frequency-dependent character of the real part.

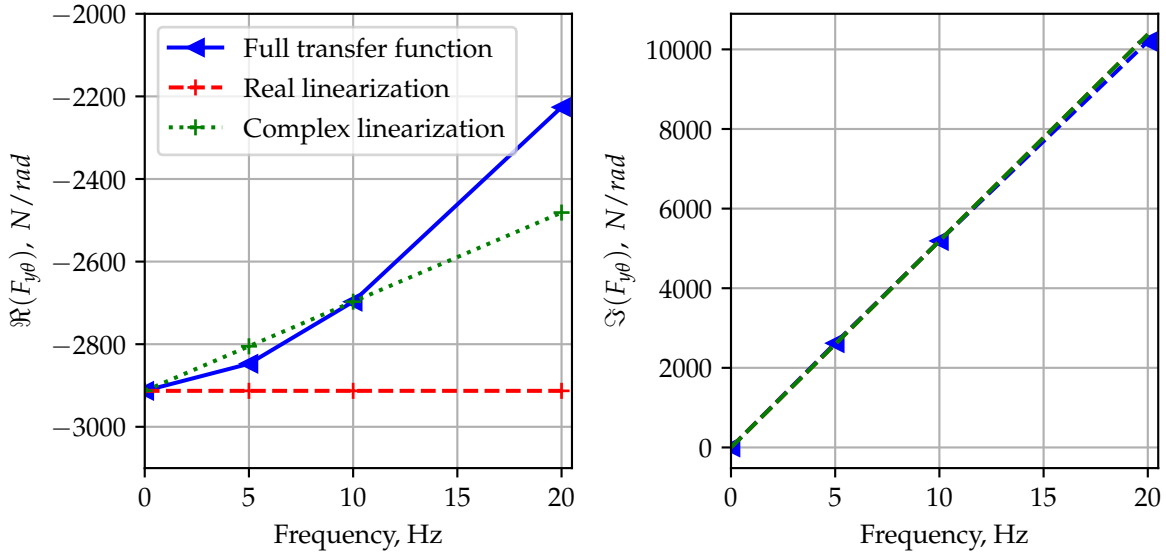

Figure 1: Complex transfer function from propeller disc pitch to lateral force. The frequency-dependent reference is shown as solid line, the real linearisation as dashed line and the complex linearization as dotted line.

The linear matrices $\underline{\tilde{K}}_{prop}$ and $\underline{\tilde{D}}_{prop}$ can be directly used in conjunction with legacy workflows, e.g., in ZAERO or MSC Nastran. Furthermore, aerodynamic derivatives can be extracted from the nondimensional form of the matrices and compared to those, e.g., from the Houbolt/Reed method, to get further insights into the aerodynamic transfer behavior. Depending on the choice of linearization, the derivatives and the aerodynamic matrices are real or complex.

2.4 Aerodynamic methods

Different methods to model the propeller aerodynamics with increasing levels of fidelity are used in this study. The methods range from quasi-steady strip theory over unsteady strip theory with and without an induced-velocity model to a mid-fidelity 3D-panel code. Induced velocities in this context denote the velocities induced on the rotor disc due to thrust and torque. The methods are a subset of the aerodynamic methods used in an earlier publication and for more details about the individual methods, the reader is referred to this work [14] and the original literature. Tab. 1 provides an overview and comparison of the different methods used.

Table 1: Comparison of aerodynamic methods used in this paper.

Method	**Blade Lift**	**Wake**	**Tip Loss**	**Comp. time**
UPM [21–23]	2D vortex lattice on camber surface + 3D source/sink panels on blade surface	Free panel wake	Included in free wake	hours
BEM+Wagner	Strip theory using airfoil polars + Wagner's function for unsteady lift lag [24]	Weighted blade element momentum theory [25, 26]	Prandtl–Glauert	minutes
Wagner	Strip theory using airfoil polars + Wagner's function for unsteady lift lag [24]	No induced velocity model	No tip loss model	seconds
Quasi-steady	Strip theory using airfoil polars	No induced velocity model	No tip loss model	seconds
Houbolt/Reed	Linearized strip theory ($C_{l\alpha}$ only) + Theodorsen's function for unsteady lift lag	No induced velocity model	Aspect ratio correction	seconds
Houbolt/Reed quasi-steady	Linearized strip theory ($C_{l\alpha}$ only)	No induced velocity model	Aspect ratio correction	seconds

3 MODELS

The following section introduces the models for the propeller and airframe used for the studies in this paper. The propeller geometry corresponds to a five-bladed, constant-speed turboprop propeller and was used in previous studies [14]. The airframe model is a generic, two-engine turboprop commuter aircraft, which is also used in a parallel study by Noël et al. [15].

3.1 Propeller

The propeller geometry for the aerodynamic time-domain calculations and the Houbolt/Reed method is shown in Fig. 2. It comprises five blades with a straight 50% chord line and symmetric NACA0008 airfoils. The geometry was used in a previous publication [14]. Details such as the chord and twist distribution can be found there. For all methods except UPM, local airfoil data has to be defined. All strips are given linear airfoil polars with a lift-curve slope of 6.5894 and no lift or moment offset. The combined polar inertia of the propeller and engine is assumed to be 6.69 kgm^2. The propeller is operated at a constant rotational speed of 1600 rpm.
For this paper, the blade pitch of the propeller blade is trimmed to obtain zero torque, equivalent to the critical windmilling conditions.

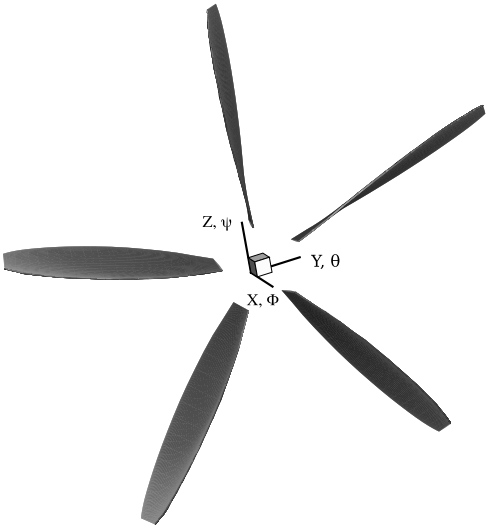

Figure 2: Propeller geometry

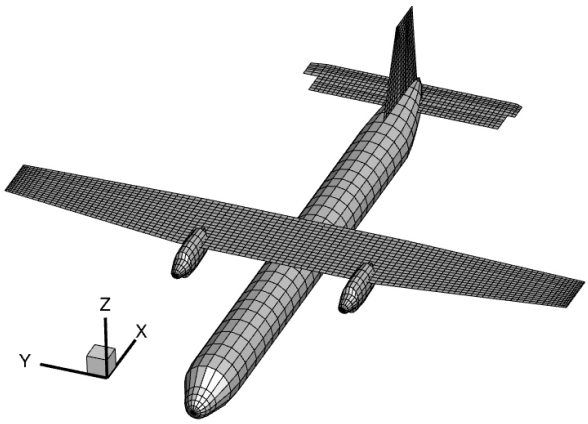

Figure 3: Aircraft geometry represented by the aerodynamic mesh of the ZAERO model

3.2 Aircraft

This paper aims to study the whirl flutter of a full, free-flying aircraft configuration. The generic model is taken from a study published in a parallel paper by Noël et al. [15] and represents a twin-engine, high-wing turboprop aircraft. The outline of the configuration can be seen from the aerodynamic panel grid in Fig. 3. The aerodynamic panel model is designed for the ZONA6 method in the commercial aeroelastic software ZAERO [19] and features panels for the lifting surfaces and bodies for the fuselage and nacelles. The structural model comprises a shell representation of the wing box and empennage structure. The fuselage consists of beam elements. The engines are modeled as rigid mass points and connected to the pylon structure using springs resembling the elastomer shock mounts. The shock mounts' stiffness is chosen low to force a whirl flutter instability within the airspeed range studied.

4 RESULTS

The results presented in this section are split into two categories. The first subsection presents the aerodynamic transfer functions of the propeller. It compares them between the different aerodynamic methods for one operating point in Fig. 4 and over the airspeed range in Fig. 5. The second subsection shows flutter results for the aircraft configuration from section 3. Fig. 6 gives an overview of the baseline flutter results using the Houbolt/Reed method, while Fig. 7 explores the impact of the different aerodynamic methods and Fig. 8 compares the linearization strategies with the original TM-method.

4.1 Aerodynamic propeller derivatives

Transfer matrices for propeller aerodynamics are computed using pulse perturbation of the propeller hub motion in translation and disc pitch motion. The identified transfer functions are also linearized into aerodynamic derivatives to compare the frequency-dependent TM-method with the real and complex linearization.

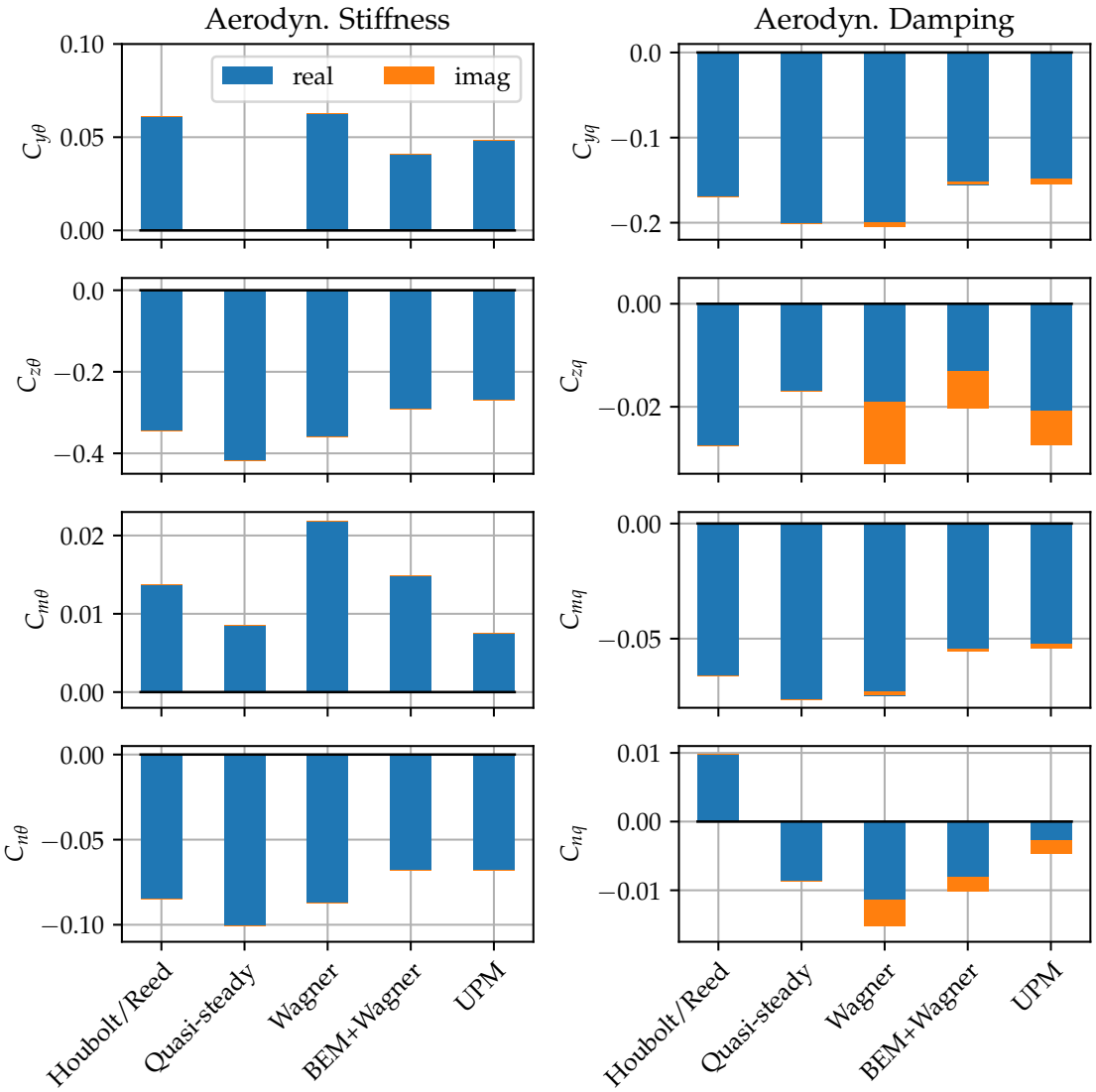

Figure 4: Aerodynamic derivatives of the propeller at V_D, calculated with different aerodynamic methods. The imaginary part for the complex linearisation is plotted as orange bar on top of the real part.

Fig. 4 shows the identified derivatives for the operating point at dive speed V_D at 142 m/s. The unique aerodynamic stiffness derivatives are shown on the left side, and the right column presents the aerodynamic damping derivatives. Due to axial symmetry, half of the derivatives are redundant (e.g., $C_{z\psi} = C_{y\theta}$) and not shown. Each plot shows the prediction for the derivative with the respective method associated with the bar. The blue part of each bar represents the real part of the derivative, and the orange part is the additional imaginary part for the complex linearization. Note the varying axis scaling when comparing between derivatives. The results reproduce the findings of an earlier paper [14, Fig. 10]. The critical derivatives for whirl flutter prediction, the destabilizing $C_{n\theta}$ and the three stabilizing components $C_{y\theta}$, $C_{z\theta}$ and C_{mq}, are reduced in amplitude when unsteady aerodynamics (going from Quasi-steady to Wagner) and induced velocities (going from Wagner to BEM+Wagner) are considered [14]. The fit between the mid-fidelity method UPM and BEM+Wagner is acceptable for these derivatives. The other four derivatives show higher deviations but have less sensitivity towards whirl flutter stability [14]. The aerodynamic stiffness derivatives are the same when comparing the real and complex linearization. This is expected, as the zero-frequency transfer functions (equivalent to the 1P hub loads) are completely real. A potential imaginary part arises for the damping derivatives, which include the transfer behavior at a higher perturbation frequency (10 Hz in this case). Interestingly, a relevant imaginary part can only be found in the smaller derivatives C_{zq} and C_{nq}. These are often even neglected in literature [4] due to their small values. The origin of these derivatives lies primarily in the unsteady aerodynamics. This can also be seen because only methods with unsteady aerodynamic modeling (the last three) show imaginary parts. The influence of this on whirl flutter is explored in Fig. 7. Compare Koch, Böhnisch et al. [14] for a more detailed comparison of the different aerodynamic methods.

To conduct flutter analyses over a range of airspeeds, the transfer functions for the propeller (either in derivative form or as transfer matrices) must be known in the whole range. Fig. 5 shows the same eight derivatives from Fig. 4, but over the velocity range from 0.25 V_D to 1.2 V_D. Only the dominating real parts are considered for this plot. The advance ratio $\mu = V_{TAS}/(\Omega R)$ is given as a second x-axis because μ varies with airspeed for the constant-speed propeller. Due to the varying advance ratio, also the aerodynamic derivatives change with airspeed. Most trends in the derivatives are similar, and only offsets occur. The only significant differences appear for the Wagner method at low advance ratios, which jumps compared to the other methods. This might be attributed to a different trim, which differs more widely between the methods in the low-speed regime, leading to different steady states and, therefore, different transfer functions. The offsets at low speeds are not investigated further as they do not impact the flutter points at high speeds. Again, a good match between the mid-fidelity method UPM and BEM+Wagner is observed, especially for the destabilizing $C_{n\theta}$ and the three stabilizing derivatives $C_{y\theta}$, $C_{z\theta}$ and C_{mq}. For most derivatives, Wagner predicts higher absolute values, which fit very well with the Houbolt/Reed method (as the assumptions are similar here). The Quasi-steady method predicts much higher derivatives for the in-phase terms (e.g., $C_{n\theta}$ and $C_{z\theta}$). The others are small or zero. Another observation from Fig. 5 is that, apart from the jump at low speeds, the derivatives change gradually with airspeed. Therefore, they are straightforward to interpolate, and only a few sampling points in the velocity range are required. Here, the five sampling points shown as markers in Fig. 5 are used at 0.25, 0.5, 0.75, 1.0, and 1.2 times V_D.

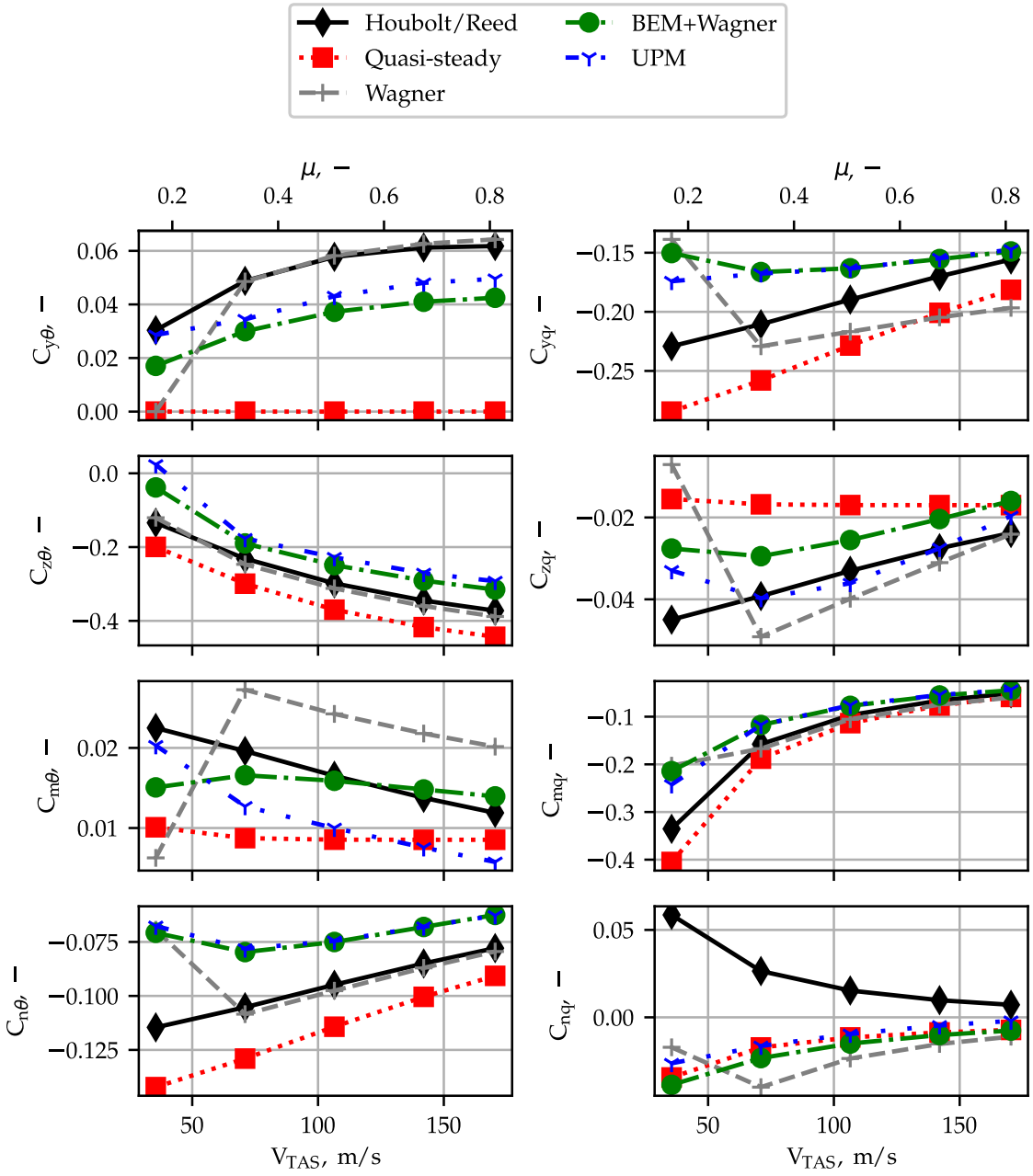

Figure 5: Comparison of aerodynamic derivatives for different airspeeds / advance ratios between the methods.

4.2 Whirl flutter results

Fig. 6 shows frequency and damping results for the generic aircraft configuration using the classical Houbolt/Reed method. They are explained as baseline results before using the identified derivatives for whirl flutter analysis. Fig. 6 presents the frequency and damping of the first 24 elastic airframe modes, excluding the six rigid body modes and the higher modes 31-50. Results are shown between zero and 170 m/s, equivalent to approx. $1.2V_D$. The rotational speed of the propeller is ramped up from zero to nominal between zero and 32 m/s to slowly introduce the gyroscopic couplings and ease mode-tracking. This leads to significant changes in the frequencies and dampings of most modes, especially those involving propeller hub motion, as the individual pitch and yaw modes merge into the whirl modes of the system under the influence of gyroscopic coupling.

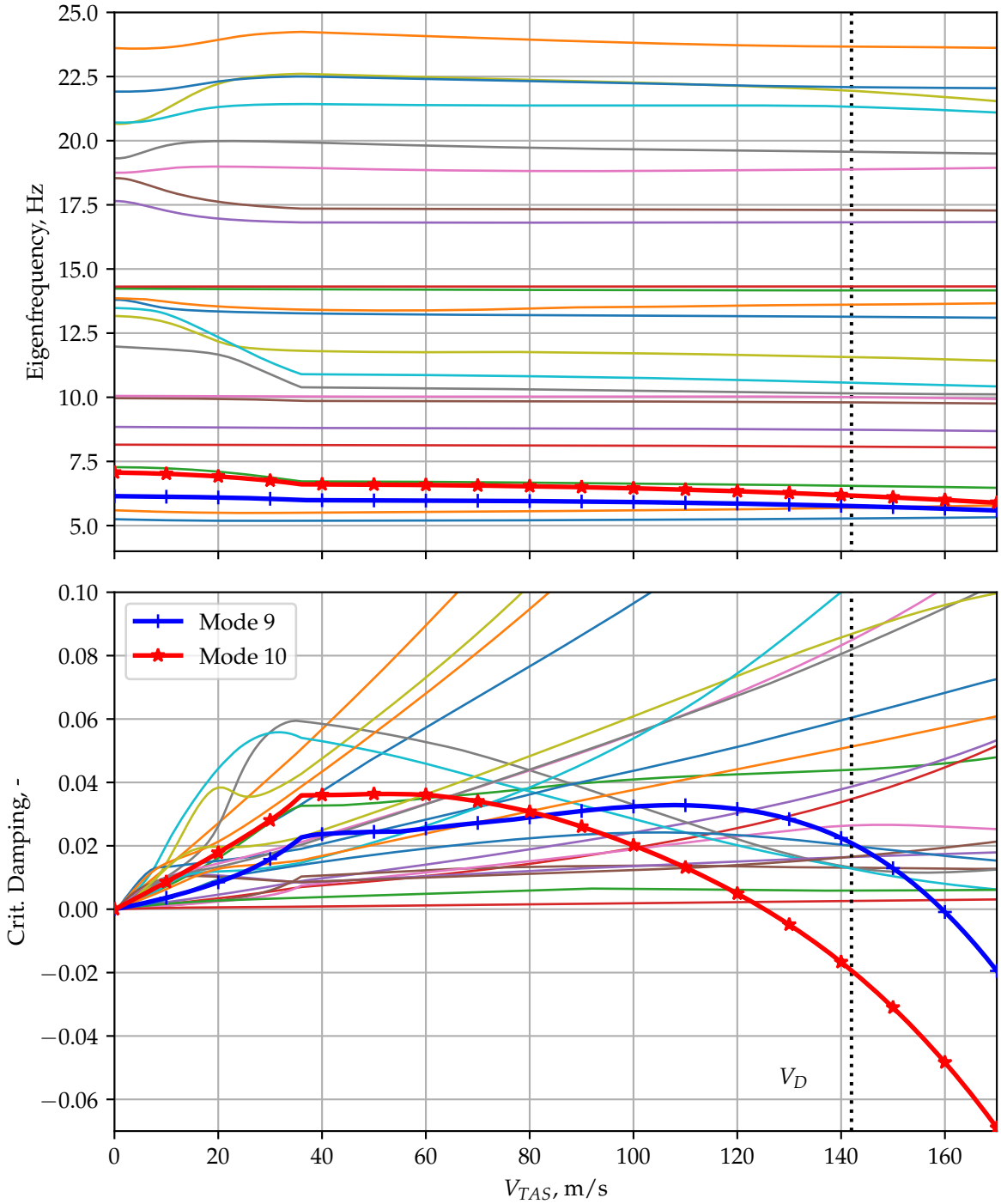

Figure 6: Frequency and damping trends of the first 24 elastic aircraft modes, calculated using propeller derivatives from the Houbolt/Reed-method

The frequency and damping trends for modes 9 and 10 are highlighted (blue is mode 9, red is mode 10). These are the two low-frequency backward whirl modes. Mode 10 involves symmetric wing torsion, engine pitch, and anti-symmetric engine yaw, leading to an in-phase whirl motion of the two propeller hubs. Mode 9 comprises anti-symmetric wing torsion, engine pitch, and symmetric engine yaw, resulting in an out-of-phase whirl motion. Both modes become unstable under the influence of the motion-induced propeller aerodynamics, as indicated by the

crossing of the zero-damping line towards negative damping values. Mode 10 becomes unstable at 125 m/s, while mode 9 becomes unstable at a higher true airspeed of 159.5 m/s. No other instability occurs in the model, and both flutter mechanisms can be characterized as classical backward whirl flutter.

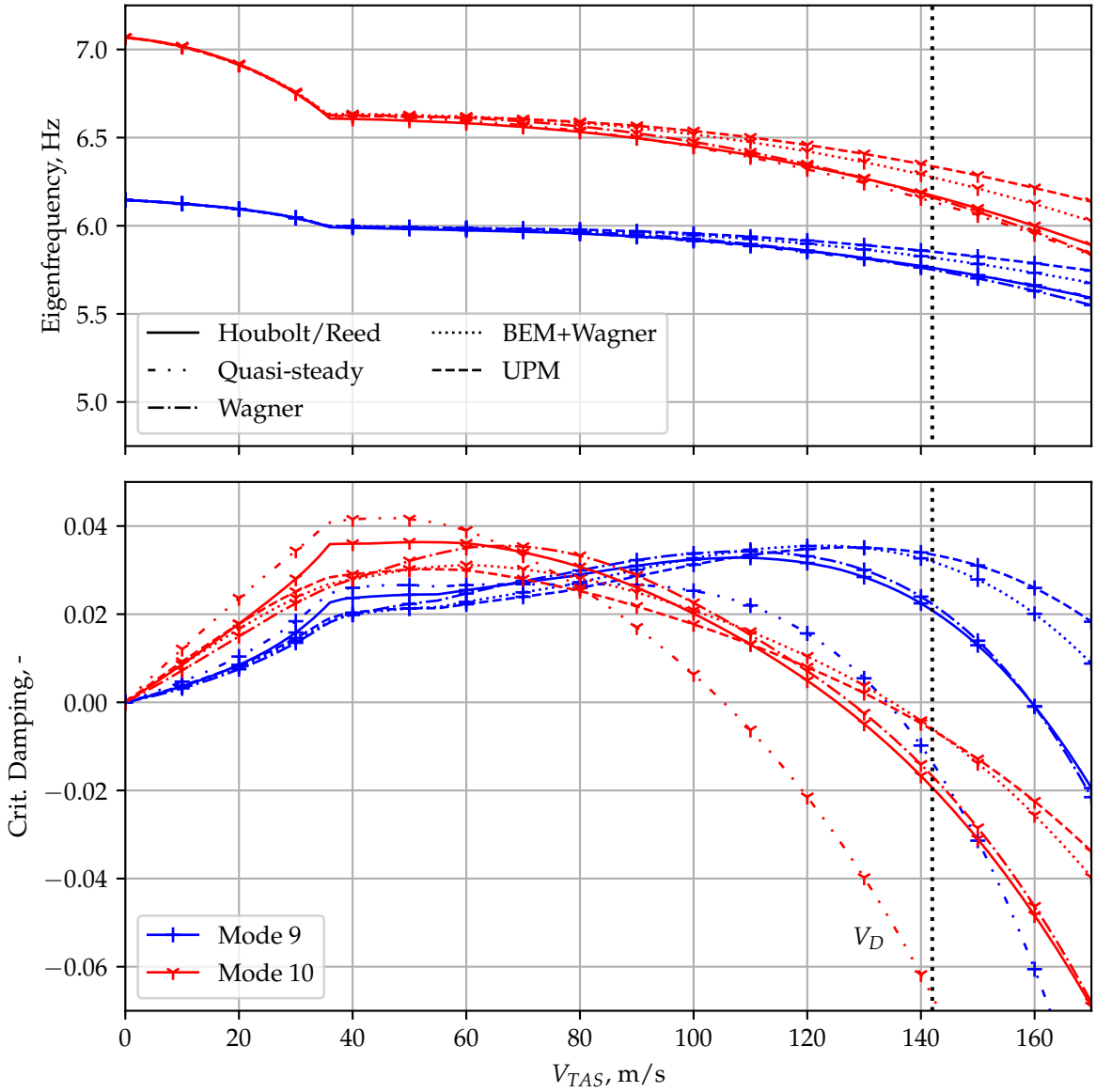

Figure 7: Frequency and damping trends of the two backward whirl modes, calculated using transfer matrices from different aerodynamic methods

Using the identified frequency-dependent transfer matrices, the influence of aerodynamic modeling on the frequency and damping trends of modes 9 and 10 are explored in Fig. 7. Only the two modes are depicted in blue and red, but trends for the five aerodynamic methods from Tab. 1 are shown, distinguishable by their line style. Differences between the five methods can be seen already in the frequency trends, especially at high airspeeds. The decrease in frequency with increasing airspeed, caused by the negative aerodynamic stiffness terms of the propeller, is higher for those methods predicting larger aerodynamic derivatives (compare $C_{n\theta}$ in Fig. 4). Quasi-steady aerodynamics predict the largest derivatives and thus lowest frequencies, and UPM and

BEM+Wagner predict the lowest derivative values and the highest frequencies. The differences are more pronounced even in the damping trends. Here also, flutter speeds are ordered according to the magnitude of the destabilizing term $C_{n\theta}$. Quasi-steady propeller modeling predicts the lowest flutter speed, while Wagner and Houbolt/Reed predictions are close together for both modes. This is expected, as both methods make similar aerodynamic assumptions (compare Tab. 1). The two more complex methods, BEM+Wagner and UPM, predict the smallest destabilizing derivative and, therefore, the higher flutter speed. This is a clearer picture compared to the findings of Koch, Böhnisch et al. [14] for the simplified pylon system. For the simplified system, the correlation between the absolute value of the predicted derivatives and the flutter stability was poor. The fact that this is clearer for the full aircraft model can be attributed to the presence of unsteady aerodynamic forces on the wing, which act dampening in this case and reduce the sensitivity of the system concerning the stabilizing derivatives. The destabilizing $C_{n\theta}$ remains the main driver behind the backward whirl instability, counteracted now by wing aerodynamics and stabilizing propeller derivatives. Thus, the absolute value of $C_{n\theta}$ is a good measure for the whirl flutter stability of this more complex configuration.

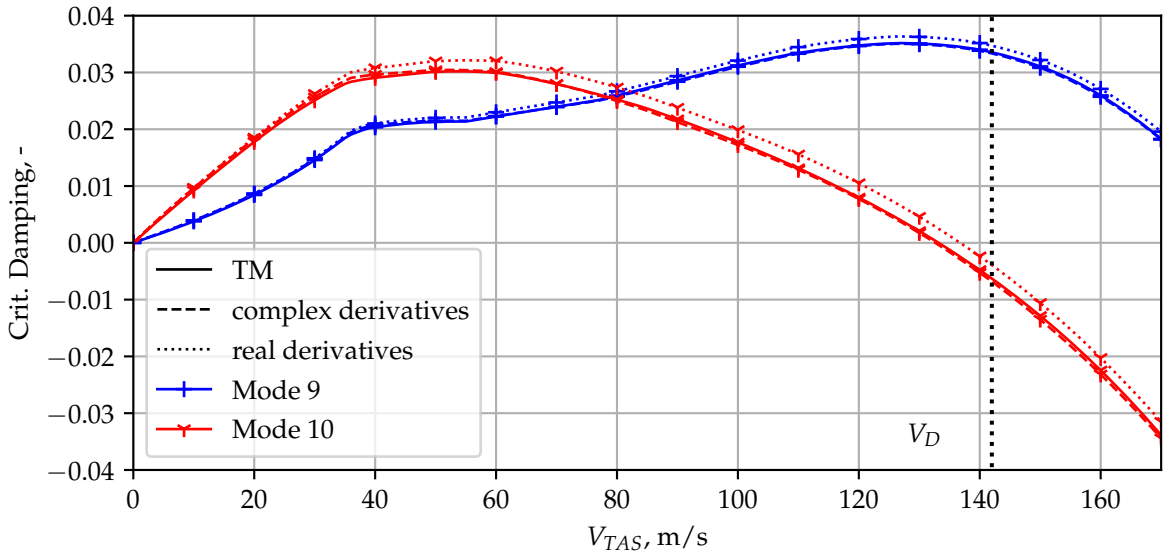

Figure 8: Damping trends of the two backward whirl modes, calculated using UPM aerodynamics for the propeller and the TM-method as well as real and complex propeller derivatives

While Fig. 7 compared results using the original TM-method for different aerodynamic methods, Fig. 8 compares the damping trends for mode 9 and 10 for UPM aerodynamics only but for the original TM-method and the two linearization methods described in section 2. The transfer matrices were linearized about the 10 Hz sample. Fig. 8 shows that the full, frequency-dependent TM-method and the linearization using complex derivatives give very similar results. Almost no difference is visible between the solid and dashed lines representing the two methods. Dropping the imaginary part of the derivatives results in a slightly more stable system, resulting in a 3.5 m/s offset in flutter speed for mode 10. The frequency trends for all three representations of the transfer matrices are equivalent and not shown.

5 CONCLUSION AND DISCUSSION

This paper presents an application of the Transfer-Matrix method to a parameter study concerning the influence of aerodynamic propeller modeling on the whirl flutter stability of a generic twin-engine turboprop aircraft. It explores the potential linearization of the frequency-dependent propeller transfer matrices into aerodynamic derivatives and its effect on the accuracy of whirl flutter studies.

Aerodynamic derivatives from five different low- to mid-fidelity methods for propeller aerodynamics are compared over a range of airspeeds. While some deviations occur in the trends at low speeds, which should be investigated more closely, the general trends at speeds relevant for whirl flutter are similar but show offsets depending on the method's fidelity. Generally, the two methods with the highest fidelity, unsteady strip theory with induced velocities from BEM and 3D panel free-wake results, show an overall good fit. This extends towards the whirl flutter predictions for a generic, twin-engine turboprop aircraft. The model studied shows two backward whirl flutter mechanisms. For both, the more advanced methods predict higher flutter speeds, correlating well with the absolute value of the prediction of the destabilizing moment coupling term $C_{n\theta}$. The impact of aerodynamic modeling on whirl flutter stability is in general relatively small compared to the influence of blade elasticity studied in a parallel publication [15].

Although complex linearisation only predicts noticeable differences in a few small derivatives compared to real linearisation, flutter results differ in terms of higher flutter speeds when dropping the imaginary part of the derivatives. This is not conservative. Hence, complex linearization should be chosen if a derivative-based description of the propeller transfer matrices is required over a full, frequency-dependent description. It remains to be tested whether the linearisation can also accurately approximate the transfer matrices and, therefore, the whirl flutter behavior in the presence of blade elasticity.

Future studies should also extend the results towards higher aerodynamic fidelity, e.g., using CFD for propeller aerodynamics. This could also lift the assumption regarding aerodynamic interaction with the wing, which was neglected in this work.

6 REFERENCES

[1] Donham, R. E. and Watts, G. A. (1997). The first case of whirl flutter. In H. I. Flomenhoft (Ed.), *The revolution in structural dynamics: the big "shake-up" in airframe design*. Palm Beach Gardens, FL: Dynaflo Press. ISBN 978-0-9659773-0-2.

[2] (2019). Certification Specifications and Acceptable Means of Compliance for Large Aeroplanes. Tech. Rep. CS-25 Amd. 23, European Aviation Safety Agency.

[3] Houbolt, J. C. and Reed III, W. H. (1962). Propeller-nacelle whirl flutter. *Journal of the Aerospace Sciences*, 29(3), 333–346. doi:10.2514/8.9417.

[4] Rodden, W. and Rose, T. (1989). Propeller/nacelle whirl flutter addition to MSC/nastran. In *Proceedings of the 1989 MSC World User's Conference*.

[5] Cecrdle, J. (2012). Analysis of Twin Turboprop Aircraft Whirl-Flutter Stability Boundaries. *Journal of Aircraft*, 49(6), 1718–1725. doi:10.2514/1.C031390.

[6] Böhnisch, N., Braun, C., Muscarello, V., et al. (2023). A Sensitivity Study on Aeroelastic Instabilities of Slender Wings with a Large Propeller. In *AIAA SCITECH 2023 Forum*.

National Harbor, MD & Online: American Institute of Aeronautics and Astronautics. doi: 10.2514/6.2023-1893.

[7] Koch, C. (2021). Parametric whirl flutter study using different modelling approaches. *CEAS Aeronautical Journal*, 13, 57–67. doi:10.1007/s13272-021-00548-0.

[8] Cecrdle, J. (2014). Influence of propeller blade lift distribution on whirl flutter stability characteristics. *Intern. J. of Mech., Aerosp., Manufact., Indust. Scien. and Engin*, 8(4).

[9] Cecrdle, J. (2019). Whirl flutter-related certification according to FAR/CS 23 and 25 regulation standards. In *Proceedings of International Forum on Aeroelasticity and Structural Dynamics (IFASD)*. Savannah, GA (USA).

[10] Wang, Z. and Chen, P. (2015). Whirl flutter analysis with propeller aerodynamic derivatives computed by unsteady vortex lattice method. In *56th AIAA/ASCE/AHS/ASC Structures, Structural Dynamics, and Materials Conference*. Kissimmee, Florida: American Institute of Aeronautics and Astronautics. doi:10.2514/6.2015-1419.

[11] Gennaretti, M. and Greco, L. (2008). Whirl flutter analysis of prop-rotors using unsteady aerodynamics reduced-order models. *The Aeronautical Journal*, 112(1131), 261–270. doi: 10.1017/S0001924000002207.

[12] Koch, C. (2022). Whirl flutter stability assessment using rotor transfer matrices. In *Proceedings of International Forum on Aeroelasticity and Structural Dynamics (IFASD)*. Madrid, Spain.

[13] Koch, C. and Koert, B. (2023). Including Blade Elasticity into Frequency-Domain Propeller Whirl Flutter Analysis. *Journal of Aircraft*. doi:10.2514/1.C037501. Article in Advance.

[14] Koch, C., Böhnisch, N., Verdonck, H., et al. (2024). Comparison of Unsteady Low- and Mid-Fidelity Propeller Aerodynamic Methods for Whirl Flutter Applications. *Applied Sciences*, 14(2). doi:10.3390/app14020850.

[15] Noël, J., Koch, C., Stickan, B., et al. (2024). Influence of blade elasticity on the whirl flutter stability of a propeller-driven aircraft. In *International Forum on Aeroelasticity and Structural Dynamics (IFASD) 2024*. Den Haag, NL.

[16] Cecrdle, J. (2015). *Whirl Flutter of Turboprop Aircraft Structures*. Elsevier. doi:10.1016/C2014-0-01800-X. ISBN 978-1-78242-185-6.

[17] Hassig, H. J. (1971). An approximate true damping solution of the flutter equation by determinant iteration. *Journal of Aircraft*, 8(11), 885–889. doi:10.2514/3.44311.

[18] Chen, P. C. (2000). Damping Perturbation Method for Flutter Solution: The g-Method. *AIAA Journal*, 38(9), 1519–1524. doi:10.2514/2.1171.

[19] ZONA Technology. ZAERO 9.3, https://www.zonatech.com/zaero.html.

[20] Hexagon. MSC Nastran 2023.1, https://hexagon.com/products/product-groups/computer-aided-engineering-software/msc-nastran.

[21] Kunze, P. (2015). Evaluation of an unsteady panel method for the prediction of rotor-rotor and rotor-bodyinteractions in preliminary design. In *41st European Rotorcraft Forum 2015, ERF 2015*, vol. 1. Deutsche Gesellschaft fuer Luft und Raumfahrt (DGLR), pp. 473–485.

[22] Yin, J. and Ahmed, S. (2000). Helicopter main-rotor/tail-rotor interaction. *Journal of the American Helicopter Society*, 45(4), 293–302. doi:10.4050/jahs.45.293.

[23] Yin, J., Van Der Wall, B., and Wilke, G. (2014). Rotor aerodynamic and noise under influence of elastic blade motion and different fuselage modeling. In *40th European Rotorcraft Forum 2014*, vol. 1. Royal Aeronautical Society, pp. 475–495.

[24] Arnold, J. and Waitz, S. (2018). Using Multibody Dynamics for the Stability Assessment of a New Double-Swept Rotor Blade Setup. In *ERF 2018 - 44th European Rotorcraft Forum*. Delft, The Netherlands.

[25] Burton, T., Jenkins, N., Sharpe, D., et al. (2011). *Wind energy handbook*. Chichester , West Sussex: Wiley, second edition ed. ISBN 978-0-470-69975-1.

[26] Smith, H. R. (2015). *Engineering models of aircraft propellers at incidence*. Ph.D. thesis, University of Glasgow, Glasgow, UK.

COPYRIGHT STATEMENT